Experimental study and numerical modeling of vibrational characteristics of a 500W PEM fuel cell stack

M. M. Mohammadi[1,*] , M. M. Barzegari[2], H. Moosazadeh[3]

[1] Faculty of Mechanics, Malek Ashtar University of Technology, Tehran, Iran.
[2] Fuel Cell Technology Research Laboratory, Malek Ashtar University of Technology, Fereydoonkenar, Iran.
[3] Department of Aerospace Engineering, Tarbiat Modares University, Tehran, 14115-143, Iran.

Article Information

Abstract

A PEM fuel cell is considered a system with a complex mechanical structure due to a large number of components with different dimensions and materials. Understanding this structure is essential to design fuel cells against dynamic loads such as shock and vibration. In this paper, modal analysis of a 500 W fuel cell with an active area of 225 cm^2 has been performed. The fuel cell has been excited in transverse and longitudinal directions, and the outputs of the sensors were recorded at several points. Using the Poly reference least-squares complex frequency-domain method, the first ten transverse and longitudinal natural frequencies and mode shapes of the model were determined. Modal analysis revealed that the lack of structural integrity, the layered structure, and the layer connection type results in the formation of mode shapes that do not match conventional predictions. Comparison of the numerical and experimental results showed a maximum difference of 15%. Furthermore, the results illustrated that changing geometrical and mechanical properties of the membrane by 45% have a negligible effect on the natural frequency of the fuel cell. Allowing for this fact will result in a significant reduction in the computational cost of large-scale fuel cells analysis.

1. Introduction

A polymer electrolyte membrane (PEM) fuel cell is an electrochemical system that converts chemical energy directly into electrical energy. In recent years, PEM fuel cells have been considered a source of new and clean energy in land, air, and sea transport, including shock and vibration environments. Structurally, the fuel cell series consists of several components, including bipolar plates, current collectors, gas diffusion

layers (GDLs), membrane electrode assemblies (MEAs), gaskets, and end plates, joined together by a clamping mechanism. When the structure is in a vibrating environment, the plates may slide over each other or leak due to local failure that can combine hydrogen and oxygen and cause a hazardous explosion in the PEM fuel cell [1]. Therefore, it is necessary to study the dynamic behavior of PEM fuel cells.

Recently, a limited number of researchers have also investigated the vibrational behavior of PEM fuel cells. Rouss et al. [2, 3] performed a vibration test on a fuel cell for aircraft applications. The experimental results demonstrated that the leakage rate variations between the beginning and the end of the test were not significant, and no problems were observed for the membrane electrode assembly or other components in the fuel cell series. Rajalakshmi et al. [4] tested a fuel cell containing 30 cells with an active surface area of 330 cm^2 . They employed graphite-based bipolar plates. The fuel cell performance was reevaluated after a vibration test, and it was observed that the fuel cell power decreased from 425 W to 410 W. Hou et al. [5] performed a shock-wave and vibration fuel cell test over 150 hours using a road simulator and a six-channel multi-axis simulator. Their results demonstrated that the fuel cell voltage fluctuated under vibration conditions and took about 20 seconds to reach the new steady state. Diloyan et al. [6] investigated the effect of mechanical vibration on the accumulation and growth of platinum particles in the fuel cell membrane. Utilizing multiple statistical comparisons, they showed that the average sizes of platinum particles corresponding to the catalyst layer varied under different mechanical vibration conditions. Deshpande et al. [7] analyzed the vibrational modes of a PEM fuel cell by the finite element method (FEM). By using the mode shapes of the PEM fuel cell, they indicated that the resonant frequencies occur at the edges of the seals, which increases the probability of leakage in the fuel cell.

Wu et al. [8] numerically investigated the vibrational response of a large fuel cell stack under severe external shock loading. They found that the location of the clamping system screws had a significant effect on the resistance of the fuel cell series to the external impact. Imen and Shakeri [9] investigated the effects of vibration loads on the performance and sealing characteristics of an open cathode PEMFC fuel cell. Using a fuel cell with an active surface area of 60 and a weight of 2.52 kg, they employed an electro-dynamic vibration generator to apply mechanical acceleration on the PEM fuel cell. The overall results showed that while the hydrogen leakage increased slightly, the mechanical vibration did not have a significant effect on PEM fuel cell performance during the test period.

With the advent of computational capabilities, numerical analyzes are widely used in the dynamic response analysis of mechanical structures. The existence of multiple components is a problem in the numerical analysis of the PEM fuel cell structure. Moreover, the complexity of the mechanical properties of the components is another difficulty that increases the computational time. Wang et al. [10] simplified the polymer fuel cell to a multilayer composite structure and then analyzed the vibrational response of a single cell. They studied the effects of thickness, modulus of elasticity, and density on vibrational modes. One of the shortcomings of their research was the lack of considering the seals' effect on the vibrational properties of fuel cells. Liu et al. [11] used the modal analysis method to study the vibration response of fuel cells using the finite element method. They separated the local modes from the main modes of the structure and investigated the effect of the clamping force on the model frequencies. Hao et al. [12] studied the mechanical integrity and gas-tightness of the fuel cell through a 200-hour road vibration test. Their experimental outcomes showed that the mechanical integrity of the fuel cell remained unchanged, but the gas-tightness reduced visibly. In addition, the power of the stack declined by

2.21 % of the initial value. Al-Baghdadi13]] studied the vibration properties of a fuel cell stack and evaluated seismic resistance under a vibration situation. They modeled natural frequencies and mode shapes of the PEM fuel cell using the finite element method. A parametric evolution was conducted to investigate how the fundamental frequency varies with changing thickness, Young's modulus, and density of every component. Moreover, they studied tuning of the natural frequencies of the PEM fuel cell to avoid high amplitude vibrations. Ahn et al. [14] measured the modal features of a PEM fuel cell to determine a principal mode that affects fuel cell performance. The frequency range of the basic responses was recognized by comparing the acceleration and internal noise in a fuel cell vehicle. By applying bending and torsional vibrations to the samples, they measured the vibration responses and obtained the frequency-dependent dynamic properties from the acceleration responses. Additionally, the influence of structural features on the vibration modes of a PEM fuel cell was studied.

The above review clearly indicates that despite the widespread development of fuel cell applications in various industries, few studies have been conducted to investigate the vibrational behavior of fuel cells. Moreover, an industrial fuel cell modal analysis has not been reported in the literature.

In the present work, the vibrational behavior of a 500 W PEM fuel cell consisting of four cells is investigated by the modal analysis method. Then, based on the experimental results, the development of a numerical model for predicting fuel cell dynamic behavior against the effects of external excitation is considered. The novelty of this study is threefold: (i) the modal properties of an industrial fuel cell are determined using experimental tests, (ii) detailed finite element simulation results of the PEM fuel cell are validated against experimental data, and (iii) solutions are proposed to simplify the numerical model of PEM fuel cells.

The rest of the study is organized as follows. Section 2 presents the experimental methodology for the modal analysis of the PEM fuel cell. In Section 3, the numerical modeling and finite element simulation of the PEM fuel cell and natural frequencies extraction are described. The simulation and experimental results are validated and analyzed in Section 4. Finally, the paper is concluded in Section 5.

2. Experimental modal analysis

To perform the modal test, the PEM fuel cell is suspended using a rubber band on a frame to provide free boundary conditions. These boundary conditions are appropriate to match the numerical results. The external excitation is applied to the fuel cell by a shaker. The shaker is fastened to a point on the PEM fuel cell and exerts a force within a specified range. To extract all the requested modes, the shakers are arranged for flexural, torsional (lateral), and longitudinal modes, respectively. Fig. 1 demonstrates different states of excitations on the PEM fuel cell.

The shaker is attached to the test specimen in such a way that a block or a metal pad sticks to the body at the excitation point, and then the shaker is attached to the gauge via a connector rod. Before attaching the shaker to the gauge, the shaker position is adjusted so that it can be connected to the test specimen without causing tension, compression, or bending of the bar. Fig. 1(d) demonstrates the connection of the shaker to the PEM fuel cell. In the modal tests, structural properties are identified by studying the behavior of data obtained at the measured points. Therefore, increasing the measured points leads to easier identification of the test specimen characteristics.
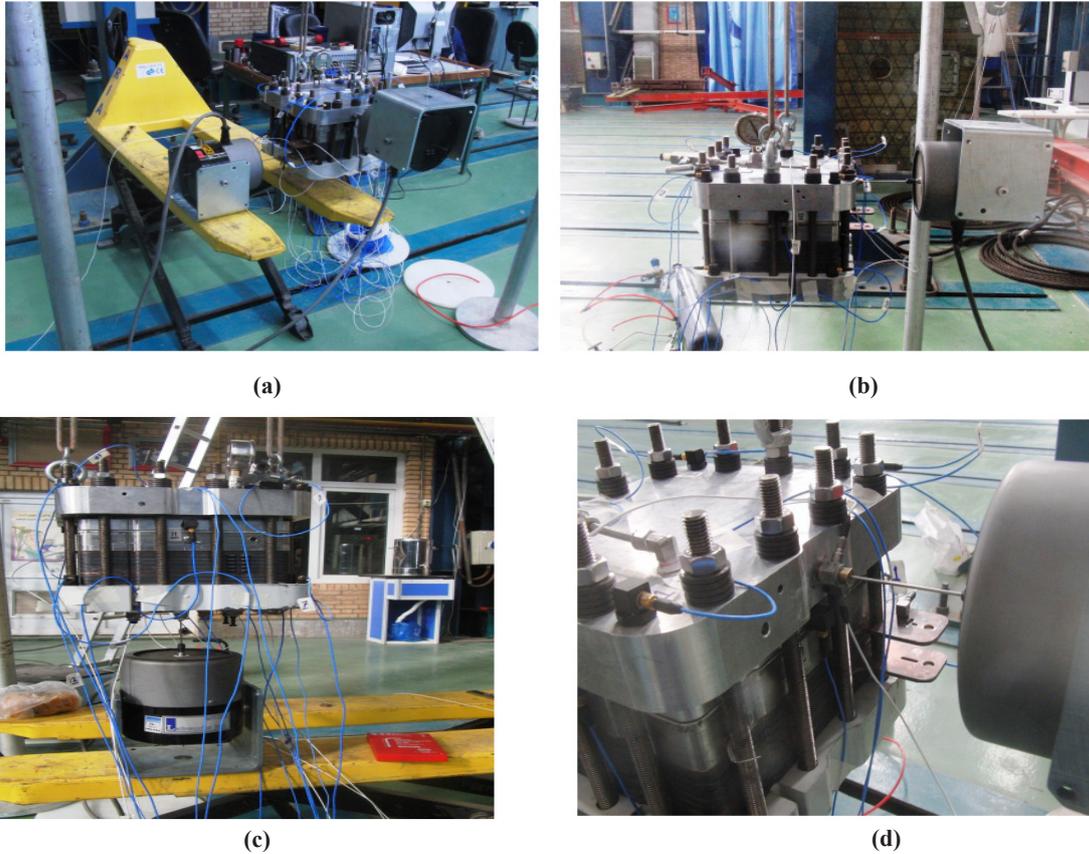
Fig. 1. Shaker excitation of the PEM fuel cell (a) in the transverse direction, (b) along two Perpendicular axes, (c) in the longitudinal direction, and (d) using a shaker bar, gauge, and metal block.

In the present test, it was not possible to connect sensors to all the components of the PEM fuel cell due to the structure and its connections. Therefore, the measured points were selected on the end plates, one of the bipolar plates, the positive current collector, and also near the excitation points. Using this arrangement, the main modes of the structure and some of its important local modes were extracted. Fifteen measured points (with the exception of the sensors near the excitation location and the current collector) were considered via three-way sensors attached to the PEM fuel cell through these points. Cartesian coordinates were used to determine the location of the measured points. The same coordinates were also used to model the test sample in the analysis software and represent the mode shapes. Fig. 2 illustrates the arrangement of the measured points.

Fig. 2. Arrangement of measured points on the test sample.

To entirely understand the system behavior during the modal test, it was necessary to obtain a physical view of the structure by estimating the behavior of the structural model using an LMS analyzer [15]. It should be noted that the LMS analyzer tested several arrangements of sensors and shaker locations to obtain the optimum model for determining the model proper-

ties of the sample. Generally, when building a software model from the test sample, the equivalent of each data point should be built, and then by drawing lines and planes, the model approximates the actual conditions. In this work, the modeling was performed with the analyzer software used for the data acquisition. Fig. 3 demonstrates the software model for the test sample.
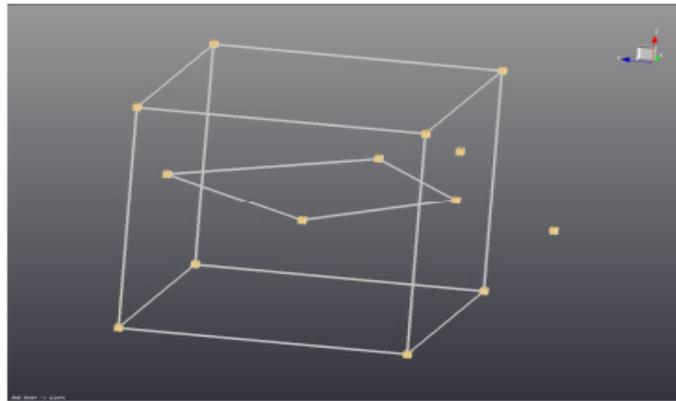

Fig. 3. Software model of test specimen.

The test layout is provided based on a predetermined design consisting of three parts: the excitation system, the data acquisition system, and the test sample. The sensors at each stage of the test are connected to the relevant points according to the designed layout.

The excitation system is made up of a load cell, a shaker, an amplifier, and connector cables. After installing the load cells and shakers, a communication circuit is established between the amplifier, shaker, load cell, and analyzer.

3. Finite element Simulation

The numerical model of a fuel cell is investigated in the following sections. The ABAQUS commercial software [16] was employed to numerically model a 500 W PEM fuel cell stack. The main components of the PEM fuel cell stack, with integrated humidifiers and water separators, are demonstrated in Fig. 4.
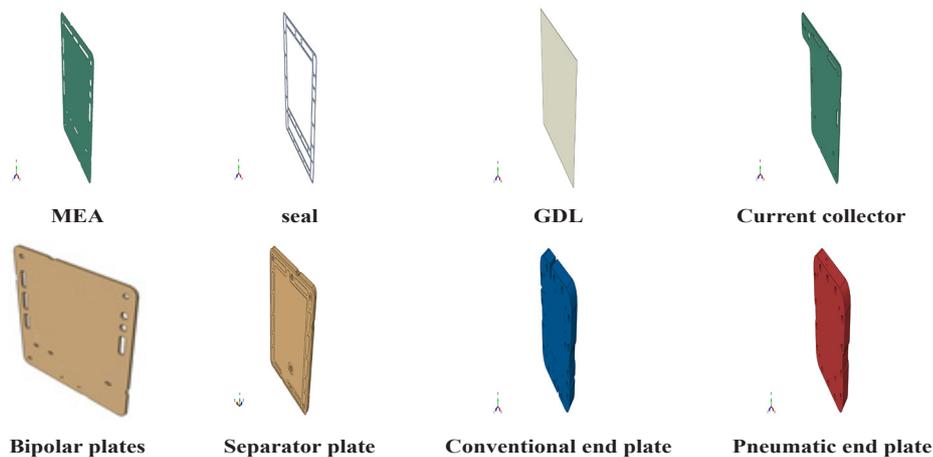

| MEA | seal | GDL | Current collector |

| Bipolar plates | Separator plate | Conventional end plate | Pneumatic end plate |

Fig. 4. The components of the desired fuel cell.

The main components of the PEM fuel cell and their mechanical properties are presented in Table 1 [17, 18].

**Table 1. Mechanical properties of fuel cell components.**

Component	Martial	(kg/m³) ρ	ν	(Gpa)E
Pneumatic end plate	Aluminum	2700	0.35	70
Conventional end plate	316 Stainless Steel	8000	0.3	200
Bipolar plates and humidifiers	Graphite-based composite	1820	0.25	3.447
MEA	[18]	2000	0.25	0.19
GDL	[18]	400	0.25	0.605
current collector	copper	8900	0.27	110

Moreover, the sealants, considered as hyperelastic material, in which the stress-strain diagram data was obtained from the uniaxial compression test are presented in Table 2 [19]. The sealant density was considered to be 1.5 g/cm³, and the Neo-Hookean model was used for numerical simulation.

Table 2. Experimental stress-strain data obtained from a uniaxial compression test of the sealant.

Normalized stress (MPa)	Normalized strain	Normalized stress (MPa)	Normalized strain
-1.07468	-0.26374	-0.12125	-0.04396
-1.29512	-0.30769	-0.27556	-0.08791
-1.54312	-0.35165	-0.44089	-0.13187
-1.81868	-0.3956	-0.63378	-0.17582
-2.18793	-0.43956	-0.85423	-0.21978

The two basic parameters in vibration and shock analysis are mass and stiffness of all components. Therefore, maintaining the properties of mass and stiffness is essential in eliminating some details of components, such as the radius of curvature or the holes that cause difficulties in component meshing. Therefore, these matters were taken into account in the finite element simulation. The assembly of the complete model of the PEM fuel cell is displayed in Fig. 5. The assembled PEM fuel cell consists of four cells with an active area of 225 cm² , two humidifier cells for humidifying oxygen and hydrogen, and two water separators. The clamping pressure is exerted on the cells by applying gas pressure to the pneumatic end plate [20].
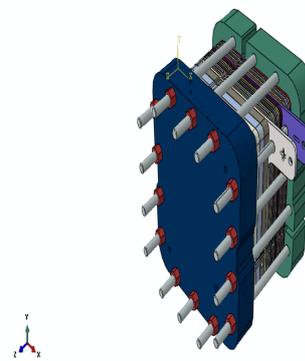
Fig. 5. Finite element model of the PEM fuel cell.

The connection between the PEM fuel cell components can be defined on the basis of contact properties in both tangential and axial directions using the software's Interaction module. Moreover, the tangential properties between the components denoted as the coefficient of friction are selected according to Table 3.

Table 3. Friction coefficient between the components of the PEM fuel cell [21].

Friction coefficient	Contact pairs	Friction coefficient	Contact pairs
0.9	Al-Sealant	1	Al-Al
0.7	Cu- Sealant	0.1	Graphite- Sealant
0.1	Graphite-Steel	0.7	Steel- Sealant
0.65	Steel-Steel	0.1	GDL- Sealant

Next, the model is partially meshed. At this stage, the meshes of the plates should be selected very carefully due to the presence of the gas flow field. To reduce the computational time, the four nodes' linear element, C3D4, was selected. Due to the geometry of the PEM

fuel cell, the fuel cell model can be greatly simplified by cutting it in the longitudinal direction. This cut results in a significant reduction in the number of mod-

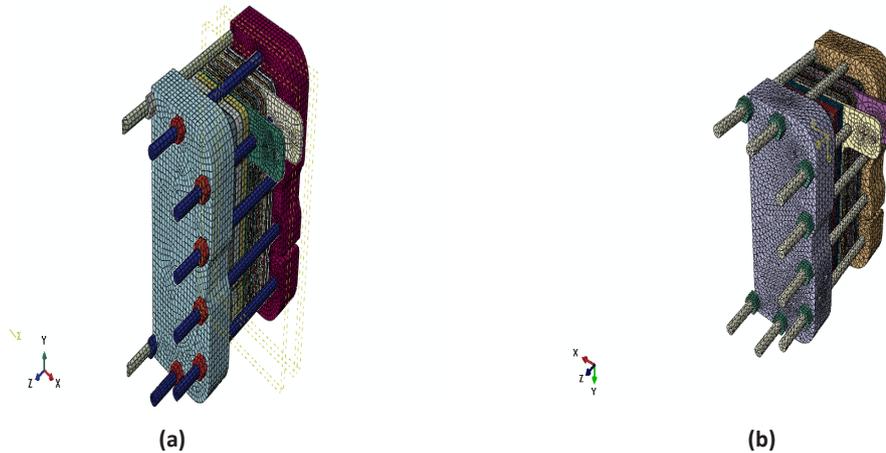el nodes. The finite element meshing created on the model is illustrated in Fig. 6.

(a)   (b)

Fig. 6. Diagrams of the model meshing with (a) regular meshes and (b) irregular meshes.

It is important to note that the finite element mesh dimensions at the contact surfaces were selected to be smaller than other parts because coarse meshing leads to a negative volume in the elements at the contact surface of the gaskets and bipolar plates. In addition, uniform modeling of the model will increase the volume of numerical computations.

we tried to obtain acceptable results by repeating the test in different situations. The high frequency of the structure's main modes caused many local modes to appear along with the two main modes. Therefore, in addition to a variety of different test procedures, several criteria were used to analyze the results. Fig. 7 demonstrates examples of the frequency response function (FRF) and coherence functions obtained from different sensors on the test sample.

4. Results and discussion

4.1. Experimental results

In this section, the experimental results are evaluated to extract the modal parameters. The modal parameter estimation methods use mathematical tools to estimate the natural frequency, mode shape, and damping coefficient. The general arrangement of these methods can be classified into two categories: time domain and frequency domain. In the present test, the PolyMax method was used to evaluate the results. Initial test results confirm that the rigidity of the test sample made it very difficult to extract the frequencies. Therefore,
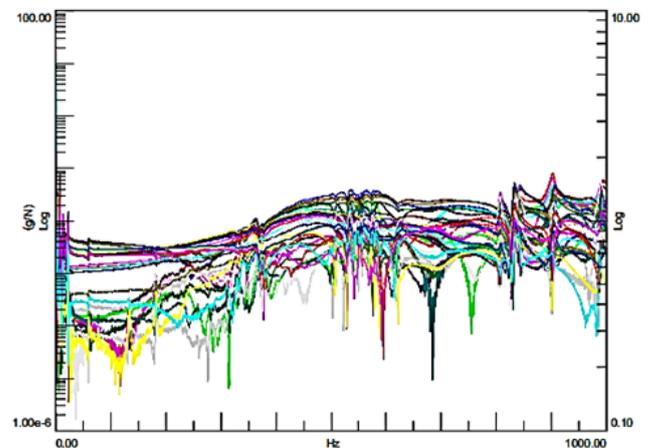

Fig. 7. Examples of the FRF and coherence functions for different test sensors.

In the present test, FRF data calculated and stored by the LMS software were employed as the test output or analysis input. The data were analyzed by this software, and the modal parameters were extracted. The FRF sum and mode identification function (MIF) [22] in one of the test steps is shown in Fig. 8. The considered frequency range is 0 to 1200 Hz. The purpose of this diagram is to examine the stability of the modal parameters in order to identify and distinguish the real or actual modes of the system from unrealistic or computational modes. Correct detection of the system's actual modes and the removal of unreal modes is one of the critical tasks of the analysis of the experimental results. To achieve this goal, the peak of the frequency response diagram, the local minimum or maximum in the MIF chart, and reasonable modality-dependent parameters (such as modal mass) were considered in addition to the stability chart.
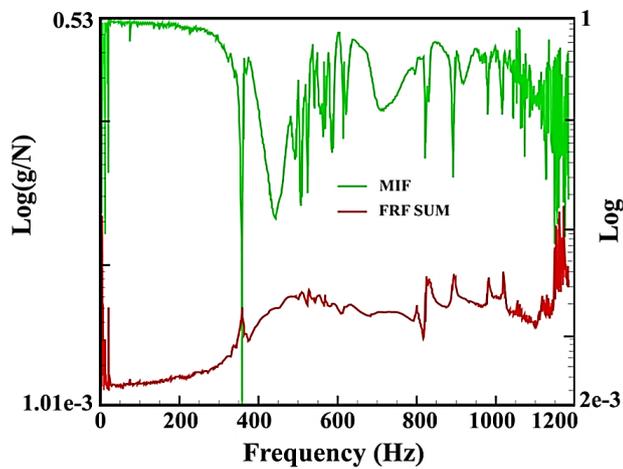

Fig. 8. The FRF SUM, MIF, and mode stability diagram in one of the test steps.

The natural frequencies and mode shapes of the PEM fuel cell are extracted by examining and comparing the results of all tests. Table 4 shows the natural frequencies of each mode.

Table 4. Natural frequencies of the PEM fuel cell.

Mode number	Natural frequency (Hz)	Description
1	242.20	Torsion mode
2	363.31	Local mode of current collector tab
3	434.24	Main bending mode of the structure
4	457.48	Flexural-torsional hybrid mode
5	466.33	Structural bending mode
6	518.80	Flexural-longitudinal hybrid mode
7	531.12	Flexural-longitudinal hybrid mode
8	623.57	Flexural-longitudinal hybrid mode
9	629.92	Flexural-longitudinal hybrid mode
10	724.14	Longitudinal mode

Fig. 9 demonstrates some of the structural mode shapes of the PEM fuel cell. Investigation of the test results found that the high rigidity of the test specimen caused the high modal frequencies. Modal analysis revealed that the lack of structural integrity, the layered structure, and the layer connection type results in the formation of mode shapes that do not match conventional predictions. As presented in Table 4, the first mode is the torsional mode. The observed torsional mode shape is mainly due to the rotation of the end plates. The second mode is the local mode, which is related to one of the current collector tabs. The third and fifth modes of the sample can be called the main structural bending modes. These modes are perpendicular to each other. The fourth mode is also a complex bending mode that seems to be affected by its side modes. Lastly, the tenth mode of the structure is the longitudinal mode. The other modes listed in Table 4 are hybrid modes.
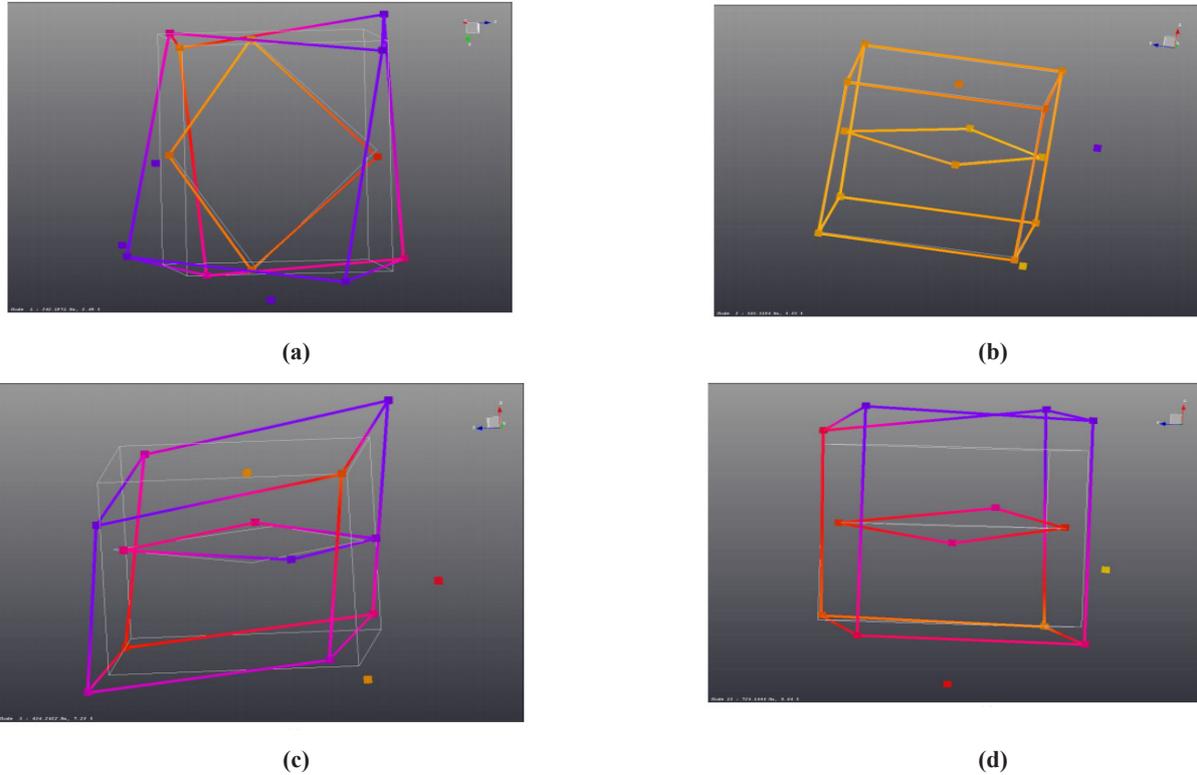
(a)

(b)

(c)

(d)

Fig. 9. Structural mode shapes of the PEM fuel cell: (a) torsional mode (242.2 Hz), (b) current collector tab mode (363.31 Hz), (c) bending mode (434.24 Hz), and (d) longitudinal mode (724.14 Hz).

4.2. Numerical results

In this section, the results of the numerical analysis of the PEM fuel cell response to external excitation in the frequency domain are evaluated. For this purpose, the displacement amplitudes of different points of the fuel cell are plotted in terms of frequency of excitation. Fig. 10(a) presents the frequency analysis of one node on the current collector tab, with an irregular mesh-

ing technique. The frequency of the current collector tab, the first flexural frequency, and some of the combined frequencies observed in the test are shown in Fig. 10(a). The results of the frequency analysis after changing the sensor location and external excitation are presented in Fig. 10(b). As shown, more frequencies of the model are observed after changing the sensor location and external excitation.
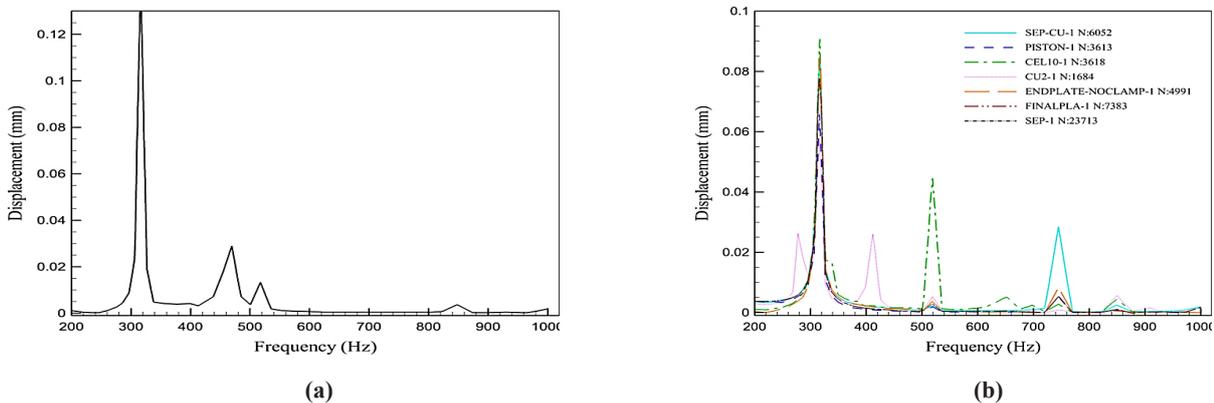

(a)

(b)

Fig. 10. FRF of the model with irregular mesh: (a) using one node attached to the current collector tab and (b) using several sensors and external excitations.

In addition, the mesh size sensitivity of FEM model was investigated. Table 5 presents the variations of the first flexural frequency according to changes in the mesh dimensions. As a result, 430,549 elements of the finite element network were selected.

Table 5. Sensitivity analysis of the finite element network dimensions.

| Number of elements	First flexural frequency (Hz)
235841	493
345231	482
430549	470
511953	470

The results of the frequency analysis with the irregular network are summarized in Table 6. As can be seen, eight frequencies of the PEM fuel cell were determined after changing the location of the response reading and the excitation location. At the observed frequencies, the torsional frequency had the highest error of 13%, which may be due to the mismatch of the model with the complete geometry.

Table 6. Comparison of simulation results using a triangular element with the modal test.

Experimental frequencies (Hz)	Numerical frequencies (Hz)	Error (٪)
242.20	275	13.5
363.31	320	11.9
434.24	410	5.6
457.48	---	---
466.33	470	0.8
518.80	510	1.7
531.12	---	---
623.57	650	4.2
629.92	680	7.9
724.14	750	3.6

The simulation results were then examined with regular networking. It should be noted that the analysis time with this networking was reduced by almost half. Fig. 11(a) shows the fluctuations created in the model with a regular grid under frequency sweep excitation. As shown in this figure, the torsional frequency of 280

Hz, the first flexural frequency of 410 Hz, and some of the combined frequencies observed in the test (520 Hz) are determined in the output signal. One of the frequencies of the current collector tabs (315 Hz) is also visible in the frequency spectrum. The results of the frequency analysis after changing the sensor location and external excitation (location and level of excitation force) are shown in Fig. 11(b). As shown in this figure, more frequencies of the model are observed after the change of sensor location and external excitation.
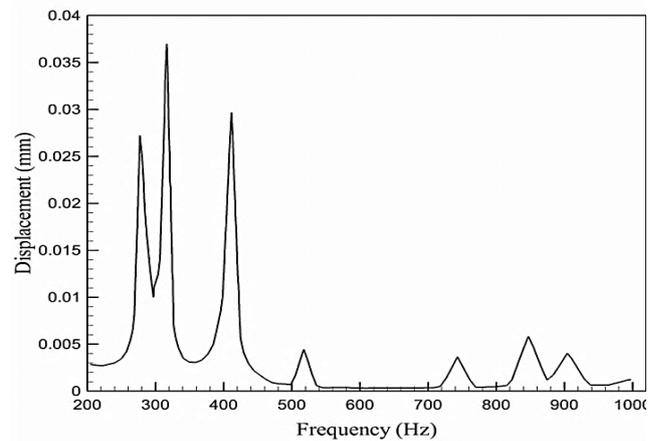
(a)
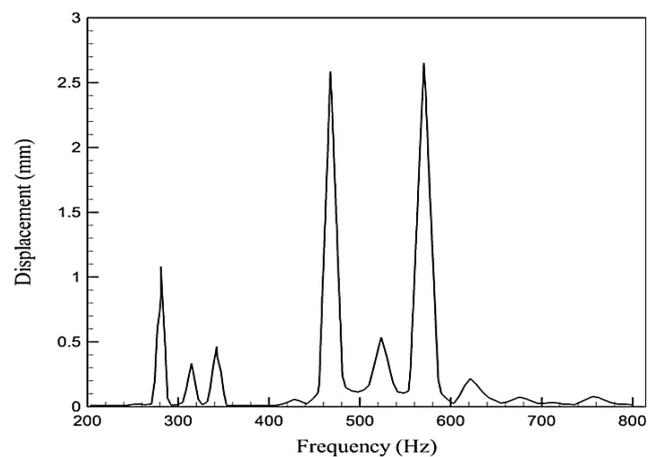
(b)

Fig. 11. FRF of the model with regular mesh using: (a) measured point connected to pneumatic end plate and (b) several sensors and external excitation.

The simulation results of the regular grid (Fig. 11) are summarized in Table 7. Accordingly, it can be concluded that except for the torsional frequency, the bending frequencies of the structure and the frequencies observed in the current collector tab are in good agreement with the frequencies observed in the experimental test. Therefore, a sufficiently detailed numerical analysis of the model can adequately cover the vibrational properties of the PEM fuel cell. Moreover, removing the gas flow field as well as half-full modeling of the fuel cell has little effect on the lateral and longitudinal frequencies of the structure while greatly reducing the amount of numerical computation. In addition, the results show that the longitudinal frequency levels of fuel cells are higher than the transverse frequencies of the model. Therefore, the transverse frequencies of the PEM fuel cell under dynamic excitation are the dominant frequencies of the model. As presented in Table 7, the obtained FEM results were validated through experimental data.

Table 7. Comparison of simulation results with a regular grid and the modal test.

Experimental frequencies (Hz)	Numerical frequencies (Hz)	Error (%)
242.20	280	15.6
363.31	340	6.4
434.24	410	5.6
457.48	425	7.1
466.33	470	0.8
518.80	520	0.2
531.12	570	7.3
623.57	615	1.4
629.92	670	6.4
724.14	758	4.7

Fig. 12(a) demonstrates the variation of the natural transverse frequency of the first model in terms of the percentage increase in the MEA thickness. As shown in this figure, increasing the membrane thickness has little effect on the natural frequency of the PEM fuel cell. The natural frequency of the fuel cell is reduced by only 3%, with a 45% change in MEA thickness. This is due to the thinness of the membrane relative to the overall dimensions of the fuel cell. The effect of the independent increase of the MEA elasticity modulus on the first natural transverse frequency is shown in Fig. 12(b). As shown in this figure, a 45% increase in the modulus of elasticity of the MEA results in an increase of 4% in the natural frequency. Accordingly, the elimination of the MEA from the fuel cell model will not have a significant effect on the frequency response of the fuel cell.
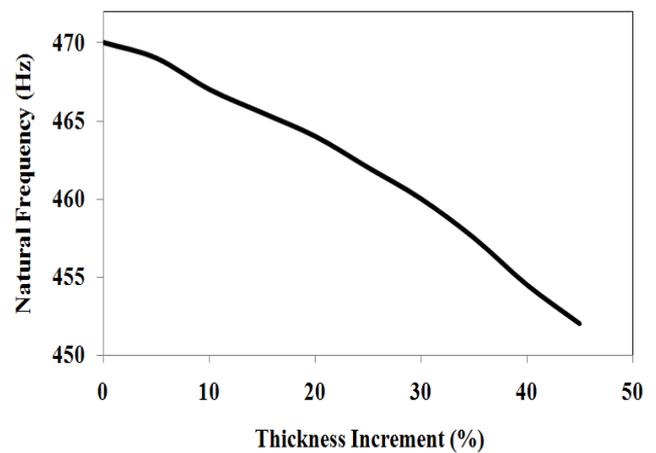
(a)
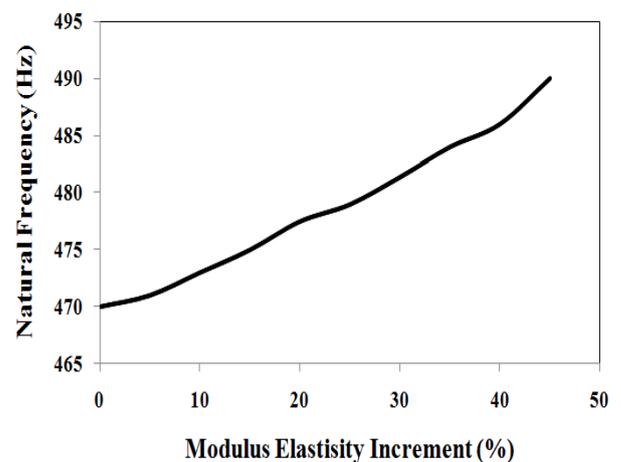
(b)

Fig. 12. The effect of MEA parameter variations on the first natural frequency of the PEM fuel cell: (a) thickness variations and (b) modulus of elasticity variations.

Table 8 presents the percent reduction of contact constraints, the percentage reduction of the finite element network, and the percentage decrease in computational cost per membrane removal. Therefore, the accuracy of the model is maintained even after removing the membrane plates, which significantly reduces the volume of numerical computations.

Table 8. Percentage reduction of call constraints, finite element network, and computational cost.

Membrane plates reduction	Contact constraints (%)	Number of elements (%)	Computational cost (%)
1	5	2	3
2	10	4	7
3	15	6	12
4	20	8	17

5. Conclusion

A polymer membrane fuel cell is considered a system with a relatively complex mechanical structure due to the existence of different plates, dimensions, and materials. Accordingly, understanding the mechanical structure of fuel cells is essential to design against dynamic loads, such as shock and impact. In this paper, a modal test of a 500 W PEM fuel cell was defined for use in numerical model validation and vibrational design. The most important research results are summarized as follows:

- Modal analysis demonstrates that the lack of structural integrity, the layered structure, and the layer connection type results in the formation of mode shapes that do not match conventional predictions.
- The bending frequencies of the structure and the frequencies observed in the current collector tab are in good agreement with the frequencies observed in the experimental modal test.
- The longitudinal frequency levels of the fuel cell are higher than the transverse frequencies of the model. Therefore, the transverse frequencies of the fuel cell under dynamic excitation are the dominant frequencies of the model.
- Increasing the membrane thickness has little effect on the natural frequency of the fuel cell due to the thinness of the membrane relative to the overall dimensions of the fuel cell.
- Removing the gas flow filled as well as half-full modeling of the fuel cell has an insignificant effect on the lateral and longitudinal frequencies of the structure while greatly reducing the amount of numerical computation.

References

[1] Wilberforce T, Alaswad A, Palumbo A, Dassisti M, Olabi A-G. Advances in stationary and portable fuel cell applications. International journal of hydrogen energy 2016;41:16509-22.

[2] Rouss V, Candusso D, Charon W. Mechanical behaviour of a fuel cell stack under vibrating conditions linked to aircraft applications part II: Three-dimensional modelling. International Journal of Hydrogen Energy 2008;33:6281-8.

[3] Rouss V, Lesage P, Bégot S, Candusso D, Charon W, Harel F, et al. Mechanical behaviour of a fuel cell stack under vibrating conditions linked to aircraft applications part I: Experimental. Internation-

al Journal of Hydrogen Energy 2008;33:6755-65.

[4] Rajalakshmi N, Pandian S, Dhathathreyan K. Vibration tests on a PEM fuel cell stack usable in transportation application. International journal of hydrogen energy 2009;34:3833-7.

[5] Hou Y, Zhou W, Shen C. Experimental investigation of gas-tightness and electrical insulation of fuel cell stack under strengthened road vibrating conditions. International journal of hydrogen energy 2011;36:13763-8.

[6] Diloyan G, Sobel M, Das K, Hutapea P. Effect of mechanical vibration on platinum particle agglomeration and growth in Polymer Electrolyte Membrane Fuel Cell catalyst layers. Journal of Power Sources 2012;214:59-67.

[7] Deshpande J, Dey T, Ghosh PC. Effect of vibrations on performance of polymer electrolyte membrane fuel cells. Energy Procedia 2014;54:756-62.

[8] Wu CW, Liu B, Wei MY, Zhang W. Mechanical response of a large fuel cell stack to impact: A numerical analysis. Fuel Cells 2015;15:344-51.

[9] Imen S, Shakeri M. Reliability evaluation of an open-cathode PEMFC at operating state and long-time vibration by mechanical loads. Fuel Cells 2016;16:126-34.

[10] Wang X, Wang S, Chen S, Zhu T, Xie X, Mao Z. Dynamic response of proton exchange membrane fuel cell under mechanical vibration. International Journal Of Hydrogen Energy 2016;41:16287-95.

[11] Liu B, Wei M, Zhang W, Wu C. Effect of impact acceleration on clamping force design of fuel cell stack. Journal of Power Sources 2016;303:118-25.

[12] Hao D, Hou Y, Shen J, Ma L. Effect of Road-Induced Vibration on Gas-Tightness of Vehicular Fuel Cell Stack. SAE Technical Paper; 2016.

[13] Al-Baghdadi MAS. A parametric study of the natural vibration and mode shapes of PEM fuel cell stacks. International Journal of Energy and Environment 2016;7:1.

[14] Ahn S, Koh H, Lee J, Park J. Dependence between the vibration characteristics of the proton exchange membrane fuel cell and the stack structural feature. Environmental research 2019;173:48-53.

[15] Mevel L, Goursat M, Basseville M, Benveniste A. Subspace-based modal identification and monitoring of large structures: a scilab toolbox. IFAC Proceedings Volumes 2003;36:1363-8.

[16] Abaqus V. 6.14 Documentation. Dassault Systemes Simulia Corporation 2014;651:6.2.

[17] Barzegari MM, Dardel M, Ramiar A, Alizadeh E. An investigation of temperature effect on performance of dead-end cascade H2/O2 PEMFC stack with integrated humidifier and separator. International Journal of Hydrogen Energy 2016;41:3136-46.

[18] Baroutaji A, Carton J, Sajjia M, Olabi A. Materials in PEM fuel cells, Reference Module in Materials Science and Materials Engineering. Elsevier; 2016.

[19] Alizadeh E, Barzegari M, Momenifar M, Ghadimi M, Saadat S. Investigation of contact pressure distribution over the active area of PEM fuel cell stack. International Journal of Hydrogen Energy 2016;41:3062-71.

[20] Barzegari MM, Dardel M, Alizadeh E, Ramiar

A. Dynamic modeling and validation studies of dead-end cascade H2/O2 PEM fuel cell stack with integrated humidifier and separator. Applied energy 2016;177:298-308.

[21] Blau PJ. Friction science and technology: from concepts to applications: CRC press; 2008.

[22] Cohen P, Cohen J, Teresi J, Marchi M, Velez CN. Problems in the measurement of latent variables in structural equations causal models. Applied Psychological Measurement 1990;14:183-96.